A NEW GLOBAL IONOSPHERE-MAGNETOSPHERE COUPLING SIMULATION UTILIZING LOCALLY VARYING TIME STEP

P. Janhunen, H.E.J. Koskinen, T.I. Pulkkinen

Finnish Meteorological Institute, Geophysical Research
P.O.B. 503, FIN-00101, Helsinki, Finland
phone: +358 0 1929557, fax: +358 0 1929539
email: Pekka.Janhunen@fmi.fi

Abstract

We present some results from a global ionosphere-magnetosphere coupling model. The model consists of a global MHD simulation box for the magnetosphere and an electrostatic ionosphere, which is coupled with the magnetosphere by field-aligned currents, the electric field, and by precipitation-dependent conductivities. The region between the ionosphere and the MHD box $1R_E < r < 3.7R_E$ is assumed to be force-free, where the magnetic field is the dipole field. In the initial state the model only contains an incoming solar wind, the Earth's dipole field (and a mirror dipole to get the magnetopause). We have run the model using real solar wind data from 29th April 1986 as well as stepwise-changing IMF. Studying the closure of Region-1 ionospheric currents reveals that these currents are closed mainly near the dayside cusp region and not in the nightside.

1. Introduction

Global MHD simulation of the Earth's magnetosphere has shown its effectiveness in giving accurate predictions for the overall geometry of the magnetosphere [Ogino, 1986, Watanabe and Sato, 1990, Tanaka, 1995, Raeder, 1995, Fedder *et al.*, 1995, for example]. However, to deal with dynamical phenomena such as auroral substorms these models have to be substantially modified. The most evident problem is that in order to simulate ionosphere–magnetosphere coupling accurately, which is presumably important for these dynamical phenomena, the global MHD model must be coupled to a relatively high-resolution ionospheric model (**Figure 1**). This sets us the requirement that the grid resolution of the MHD model must also be relatively good near the Earth, which is not the case with conventional global MHD codes using stretched Cartesian or equidistant Cartesian grid.

Meeting the high near-Earth resolution requirement is not too difficult by itself, for it can be accomplished by constructing a strongly nonuniform spatial grid. The real difficulty comes from the Courant-Friedrichs-Lewy constraint for the timestep, which states that the timestep must be shorter than the fastest possible wave travel time across a grid cell. The fastest wave speed in the near-Earth region (low-beta plasma) is approximately equal to the local Alfvén speed, which is proportional to the magnetic field. In this study we employ a sphere of radius $3.7R_E$ to represent the inner edge of the MHD equations. At this shell the dipole field is roughly 1000 nT. If the plasma density is 1 cm^{-3}, the Alfvén speed is about 20000 km/s. Taking a grid spacing of 0.1 R_E, which represents "good" resolution gives us a timestep of 0.03 s or less. In practice the minimum timestep may be even smaller, of the order 0.01 s. To simulate one hour would thus require several hundred thousand timesteps, which is more than we can afford with current supercomputers, and even then the effective ionospheric resolution is not better than about 100 km. Because of the strong dipole field, the simulation of the Earth's magnetosphere is in this sense numerically more challenging than, for example, simulating solar wind flow past a comet.

However, from the previous consideration we see that the very short timesteps are required only in the most near-Earth layers of grid points. In more distant regions the dipole field quickly becomes much smaller and correspondingly the timestep can be made larger. Thus we were led to consider algorithms which use a locally varying timestep, and indeed found a reasonably efficient method to do the necessary bookkeeping and interpolation tasks in both space and time.

2. Simulation model

2.1. Choice of the grid type

In non-global simulations a uniform rectangular grid (**Figure 2**) can sometimes be used, which is a major simplification. In global studies one must use a nonuniform grid, though. We have considered two possibilities (**Figure 2**): a stretched Cartesian grid and a hierarchical cubic grid (octogrid). The stretched Cartesian grid is easy to program (almost as easy as a uniform grid) and the resulting program can be easily vectorized and parallelized. The hierarchical cubic (HC) grid, on the other hand, gives a more economical use of grid points. Accord-

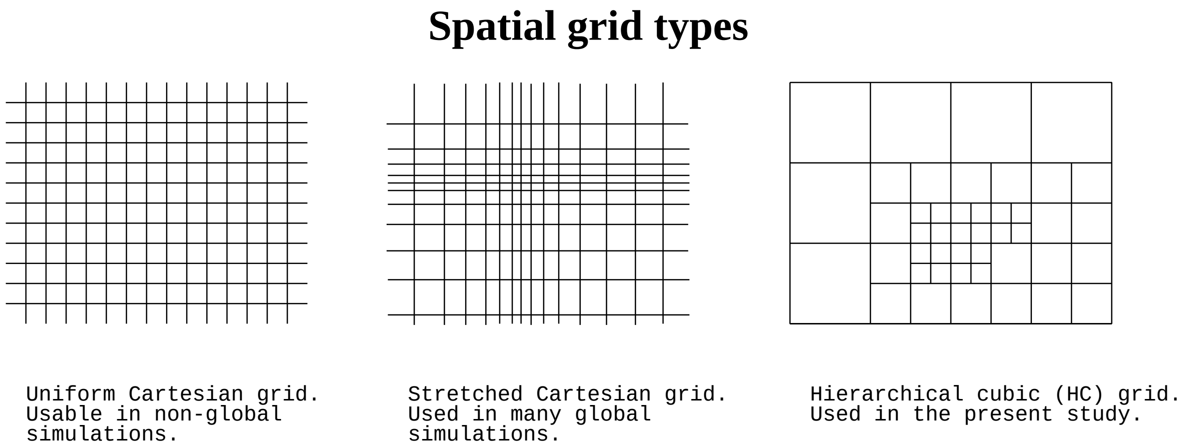

Figure 2: The three basic grid types. The HC grid (rightmost) is the one used in the present study.

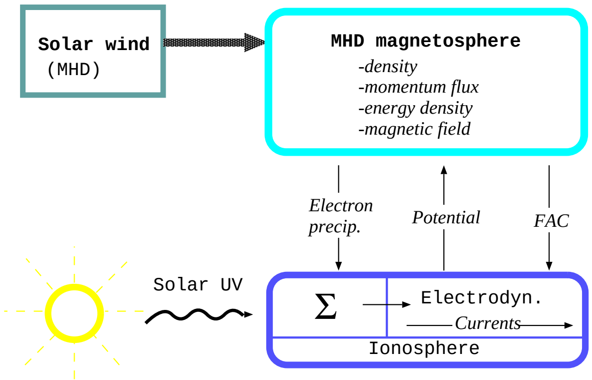

Figure 1: The overall structure of the GUMICS model

ing to our numerical experimentation the benefits of the HC grid clearly outweight the benefits of the stretched Cartesian grid. The benefits of the HC grid are further amplified by the use of a locally varying timestep (discussed below). Even the HC grid wastes some grid points because all grid sizes are powers of two. However, the hierarchical nature of the grid enables one to do interpolations (lookups) fast, in $O(log N)$ time, and it is for this reason that we have decided not to consider non-hierarchical (fully irregular) grids, which could be theoretically close to optimum from the grid cell econonomy point of view. Even though interpolations at an arbitrary point are not required in the simulation itself, they are required in any viewing or post-processing of the results so it is highly desirable that this operation works relatively fast.

We use an analytic function of x, y, z as the grid point density function. In the near-Earth region the function is such that the grid spacing is proportional to $r^{3/2}$. This behavior ensures that the number of grid cells threading a magnetic flux tube stays approximately constant along the flux tube. We set extra grid densifications also at the dayside magnetopause and the tail current sheet regions, to model dynamic processes (e.g., reconnection) as accurately as possible. We also use a bit more dense grid on the nightside than on the dayside. The model is certainly quite flexible and one can "tune" the code for different purposes by just modifying the density function.

The spatial differencing is carried out using the finite difference approach with second-order accurate formulas. At points where the grid point density changes the second-order accurate formulas become rather complicated. The number of coefficients needed to compute each spatial derivative will also vary from point to point. To save time we precompute the derivative coefficients in tables during program initialization.

The differencing scheme employed in the version is the Lax-Friedrichs method [Press *et al.*, 1992, for example] used on the semiconservative form of the MHD equations [Raeder, 1995, for example]:

$$\frac{\partial\rho}{\partial t} = -\nabla\cdot(\rho\mathbf{v}), \qquad \frac{\partial}{\partial t}(\rho\mathbf{v}) = -\nabla\cdot(\rho\mathbf{v}\mathbf{v} + P\mathrm{I}) + \mathbf{j}\times\mathbf{B},$$

$$\frac{\partial}{\partial t}\left(\frac{P}{\gamma-1} + \frac{1}{2}\rho\mathbf{v}^2\right) = -\nabla\cdot\left[\left(\frac{\gamma}{\gamma-1}P + \frac{1}{2}\rho\mathbf{v}^2\right)\mathbf{v}\right] + \mathbf{j}\cdot\mathbf{E},$$

$$\frac{\partial\mathbf{B}}{\partial t} = -\nabla\times\mathbf{E}, \qquad \nabla\cdot\mathbf{B} = 0,$$

$$\mathbf{E} + \mathbf{v}\times\mathbf{B} = 0, \qquad \mathbf{j} \equiv \frac{1}{\mu_\circ}\nabla\times\mathbf{B}.$$

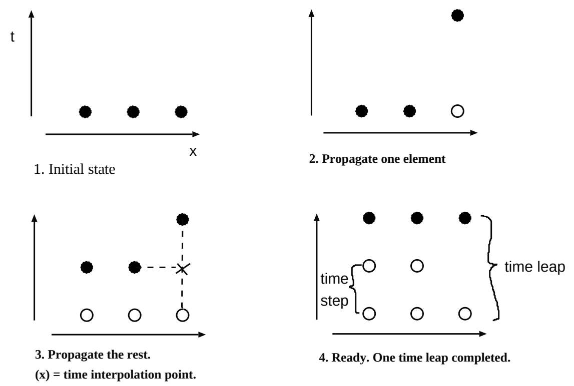

Figure 3: Principle of the locally varying time stepping in one-dimensional case.

Numerical experimentation indicates that the method is stable if the numerical diffusion is unity (i.e., the basic Lax-Friedrichs value) for the density ρ, momentum flux $\rho\mathbf{v}$ and the plasma energy density, but for the magnetic field the diffusion may be set to a small positive value (0.05) without risking stability. This means that although the code is rather diffusive in the gasdynamical part, the numerical resistivity is nevertheless small.

2.2. Time stepping

Explicit finite-difference and finite element methods require that the timestep obeys the Courant-Friedrichs-Lewy (CFL) condition everywhere: $\Delta t < \Delta x / \max v_s$, where $\max v_s$ is the maximum local signal speed. In this study we use $\Delta t = 0.4\Delta x / \max v_s$. In case of MHD equations, $\max v_s$ obeys the relation $\max v_s \le |\mathbf{v}| + \sqrt{c_s^2 + v_A^2}$, where c_s is the fluid sound speed, $c_s = \sqrt{\gamma P/\rho}$, and v_A is the Alfvén speed, $v_A = |\mathbf{B}|/\sqrt{\mu_0 \rho}$. Because the Alfvén speed is high in the near-Earth region, the timestep becomes very small there. The problem becomes even more pronounced if we use (as we do) a strongly nonuniform grid, because then the grid spacing Δx is small in the same region where v_A is large. In conventional simulations the same timestep Δt is used everywhere in the grid. In the present simulation we let the timestep vary from grid point to grid point.

For our specific grid point density function, we estimated that using the HC grid and locally varying timestep (**Figure 3**) provides about 25-fold increase in code performance as compared to using an equivalent stretched Cartesian grid and global time stepping. "Equivalent" stretched Cartesian grid here means that the grid has been constructed as optimal grids obeyingh the same density function.

2.3. Ionospheric equations

The ionospheric equations are similar to those developed in [Janhunen and Huuskonen, 1993] and also in [Janhunen *et al.*, 1995] except that the geometry is now global:

$$-\nabla \cdot \left(\Sigma_P \nabla \Phi_i + \Sigma_H \hat{\mathbf{b}} \times \nabla \Phi_i \right) = j_{\parallel}^{(i)} \sin I, \qquad (1)$$

where I is the magnetic inclination angle. The height-integrated Pedersen and Hall conductivities Σ_P and Σ_H are computed from expressions of the form $\Sigma_{P,H} = \int dh F_{P,H} n$, where the quantities $F_{P,H}$ depend only on the neutral atmosphere model and the electron density n is followed in 3D grid using the continuity equation

$$\frac{\partial n}{\partial t} = q - \alpha n^2$$

where q is the ionization production rate caused by electron precipitation. It depends on the magnetospheric source plasma density and temperature, which are obtained from the MHD variables, as well as the field-aligned potential drop $\Delta\Phi \equiv \Phi_m - \Phi_i$, $q = Q(\rho, T, \Phi_m - \Phi_i)$. $Q(.,.,.)$ is a precomputed function (for details, see [Janhunen and Huuskonen, 1993]). We assume that a linear relation holds between the field-aligned current $j_{\parallel}^{(i)}$ and the potential drop,

$$j_{\parallel}^{(i)} = K(\Phi_m - \Phi_i) \qquad (2)$$

where K = const (the Lyons-Evans-Lundin constant) is equal to 10^{-9} mho m^{-2}. The computational cycle is such that first the field-aligned current (FAC) is computed from its MHD definition, $j_{\parallel} = (\nabla \times \mathbf{B})/\mu_\mathrm{o}$. Then the FAC is mapped to the ionospheric plane by multiplying by the magnetic field ratio and used as a source term for the elliptic equation [Equation(1)], which yields the ionospheric potential Φ_i. Using (2) we then obtain the magnetospheric potential Φ_m (at the ionospheric plane at first) as $\Phi_m = j_{\parallel}^{(i)}/K$. After Φ_m is mapped to the magnetosphere (to the $r = 3.7 R_E$ shell) we compute the associated $\mathbf{E} \times \mathbf{B}$ perpendicular velocity and use it as a boundary condition for the MHD equations.

3. Run with real IMF data

We use the 29th April, 1986 event as a real-world test of our code. The IMF data (IMP 8) for this event is shown in **Figure 4**. The B_z is mainly positive during the event, but there is a short negative excursion just before 03 UT. In reality a substorm onset took place at 0257 UT [Pulkkinen *et al.*, 1992].

The simulation does not produce an identifiable substorm. However, it demonstrates clearly how the

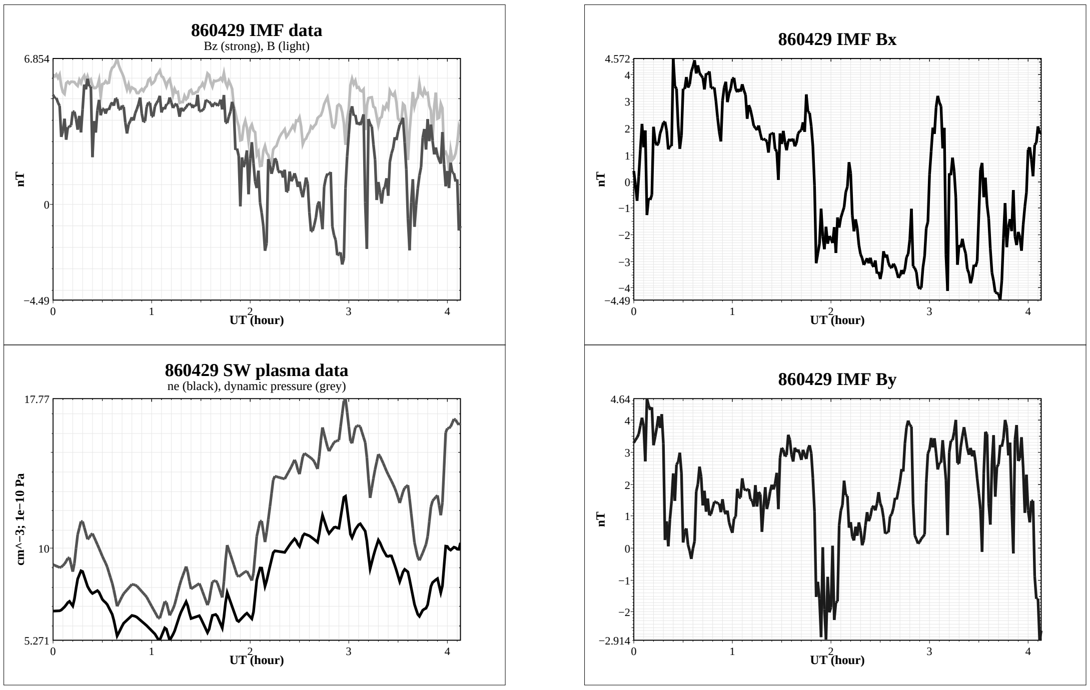

Figure 4: Left upper panel: IMP 8 IMF B_z, $|\mathbf{B}|$ data for the event used in this study (29th April 1986, 00 - 04 UT). Left lower panel: Solar wind density and dynamic pressure. Rigth upper panel: IMF B_x. Right lower panel: IMF B_y.

overall geometry of the magnetosphere changes many times under the changing solar wind conditions. The difference between the real-IMF run and another run where the solar wind is temporally constant (data not shown) is very evident. Notice that the solar wind variations are rapid enough so that many variations occur during the time it takes for the solar wind to travel through the simulation box, thus the far tail may experience completely different IMF conditions than the midtail, for example, which is probably a major source for the complicated behavior seen in the real-IMF case.

One can put forward many explanations why a substorm onset does not occur in the simulation. What we think is the most probable reason is that in this first locally varying timestep version, we are using a simple differencing scheme (the Lax-Friedrichs method) which contains more numerical diffusion (dissipation) than more sophisticated methods. (However, as was mentioned above, the numerical diffusion appears mainly in the continuity, momentum and energy equations while the numerical resistivity is small.) One clearly identifiable effect of numerical diffusion is that plasma can escape from the closed field lines by the following process: the plasma first spreads because of diffusion from closed to open field lines in the perpendicular direction and then escapes to the solar wind along the open flux tube. This prohibits the formation of sharp gradients at, e.g., that plasmasphere boundary, which may be important for substorm triggering.

4. Region-1 current closure

The question what is the closure path of Region-1 (or Region-2) field-aligned currents is difficult to study observationally so our simulations may be helpful. We have traced the lines of current density starting from the ionosphere. An example is shown in **Figure 5**. In that case we have followed ten current lines, which form a small circle at the ionospheric plane, centered at 69° magnetic latitude at 18:00 local time, which is close to the maximum intensity of the eveningside FAC. Changing the footpoint in the ionosphere along the R1 "banana" of course would alter the closure path somewhat, but not dramatically. Likewise, the corresponding figure under real IMF data would be qualitatively similar, only some dawn-dusk asymmetry in the current path would be seen due to nonzero IMF B_y.

Our result seem to be at least qualitatively in agreement with the results of [Tanaka, 1995], who used a different kind of numerical method to solve the MHD equations. These results may be of importance e.g. when trying to understand the response time of the Region-1 current system and the associated particle precipitation to solar wind variations. Our dayside closure path should enable a faster response time

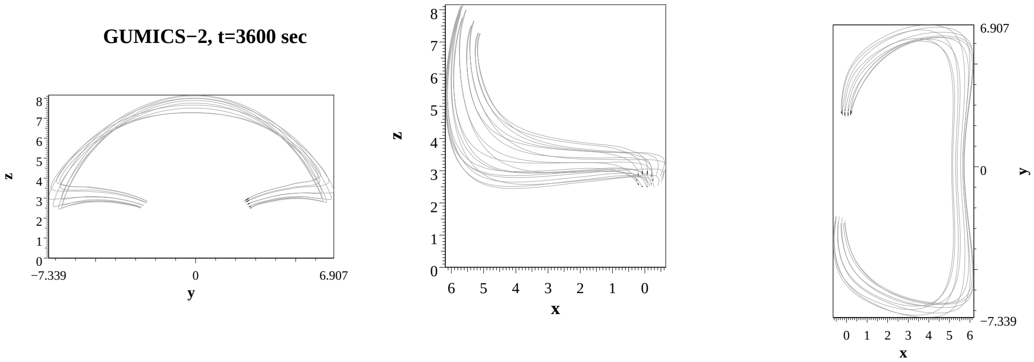

Figure 5: The X, Y and Z projections of the path of the main Region-1 current

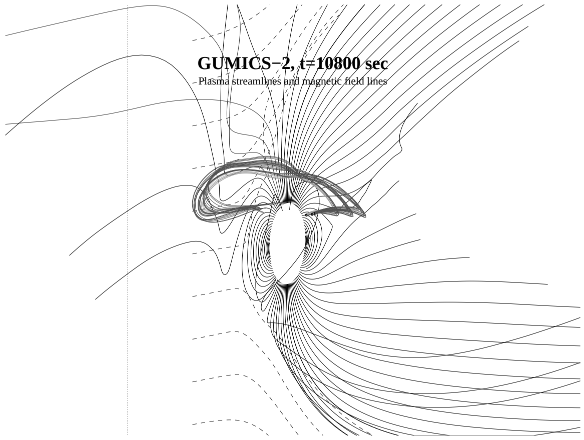

Figure 6: Event 860429, $t = 10800$, Oblique front view of the plasma streamlines (dashed), magnetic field lines (solid) and some Region-1 field lines, which originate from the eveningside ionosphere, pass through the $Y = 0$ plane near the cusp and follow an approximately symmetric path when arriving back to the ionosphere on the morningside.

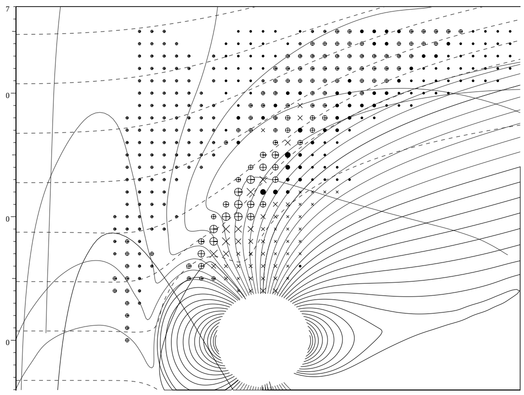

Figure 7: Event 860429, $t = 10800$, Map of the origin of $Y = 0$ crossing current. Crosses: current goes to ionosphere, Black circles: current goes back through $Y = 0$ plane on the nightside (tail current loop), Open circles: current goes back through $Y = 0$ plane on the dayside (Chapman-Ferraro current loop).

than a nightside one.

In **Figure 6** we have traced three bunches of current lines, all originating from 70 ° magnetic latitude but the longitudes given by 70°, 90° and 110°, respectively. We see that all bunches follow qualitatively similar closure paths.

One can also ask where the current that crosses the noon-midnight meridian (the $Y = 0$ plane) at a particular point goes. In **Figure 7** we have classified points on the $Y = 0$ plane in three types according to the topology of the corresponding current line. Crosses represent current lines that go to the ionosphere. The near-Earth $Y = 0$ plane is filled with these currents; the most intense currents pass through the $Y = 0$ plane near the cusp at about ($X = 3R_E, Z = 8R_E$). These are mainly Region-1 currents. Black circles correspond to currents that pass through the $Y = 0$ plane for a second time on the nightside region ($X < 0$). In the equatorial plane these correspond either to the cross-tail current or to the partial ring current (which are topologically similar). Finally, open circles correspond to currents that pass through the $Y = 0$ plane for a second time on the dayside. These are Chapman-Ferraro current loops, which are loops going around the cusp. Currents with $j_y > 0$ have been excluded from **Figure 7**. The data is from the real-IMF case at a moment of negative B_z, and consequently dayside reconnection is also evident in **Figure 7**.

5. Summary and conclusions

We have presented a new algorithm for the coupled solar wind – magnetosphere – ionosphere system, which relies on locally varying timestep and hierarchical cubic grid to propagate the MHD equations. We pointed out that this technique is the key to reaching satisfactory ionospheric resolution, which is necessary (but not sufficient) for simulating highly dynamical near-Earth phenomena such as substorms. Using the simulation we studied the closure path of the Region-1 current system and found that the current which leaves the ionosphere as Region-1 current crosses the $Y = 0$ plane near the cusp. This result applies for the bulk of Region-1 current and seems to be rather insensitive to numerical factors such as number of grid points.

A limitation of our first locally varying timestep simulation is that it contains apparently too much numerical diffusion to produce sharp pressure and density gradients and substorms. However, we demonstrated the functioning of the model using real IMF data (29 April 1986) and compared the results with constant solar wind cases. The magnetospheric configuration was much more complicated in the real-IMF case, not only because of nonzero IMF B_y etc. but also because the temporal variations of the solar wind are fast compared to the travel time (45 minutes) across the simulation box.

We are currently running a new version of the code which uses a more sophisticated discretization scheme (the finite volume method with a linearized Riemann solver). As we were able to produce auroral activations in our previous "semiglobal" studies [Janhunen *et al.*, 1995] using essentially the same equations as the current model, we think it is realistic to expect that by reducing numerical diffusion we can reproduce these semiglobal results in the global framework.

References

Fedder *et al.*, 1995. Fedder, J. A.; Lyon, J. G.; Slinker, S. P.; Mobarry, C. M., Topological structure of the magnetotail as a function of interplanetary magnetic field direction, J. Geophys. Res., 100, 3613–3621, 1995.

Janhunen and Huuskonen, 1993. Janhunen, P. and Huuskonen, A., A numerical ionosphere-magnetosphere coupling model with variable conductivities, J. Geophys. Res., 90, 9519–9530, 1993.

Janhunen *et al.*, 1995. Janhunen, P., Pulkkinen, T.I., and Kauristie, K., Auroral fading in ionosphere-magnetosphere coupling model: Implications for possible mechanisms, Geophys. Res. Lett., 22, 2049–2052, 1995.

Pulkkinen *et al.*, 1992. Pulkkinen, T.I., Baker, D.N., Pellinen, R.J., Büchner, J., Koskinen, H.E.J., Lopez, R.E., Dyson, R.L., and Frank, L.A., Particle scattering and current sheet stability in the geomagnetic tail during the substorm growth phase, J. Geophys. Res., 97, 19283–19297, 1992.

Raeder, 1995. Raeder, J.; Walker, R. J.; Ashour-Abdalla, M., The structure of the distanct geomagnetic tail during long periods of northward IMF, Geophys. Res. Lett., 22, 349–352, 1995.

Tanaka, 1994. Tanaka, T., Finite volume TVD scheme on an unstructured grid system for three-dimensional MHD simulation of inhomogeneous systems including strong background potential fields, J. Comp. Phys., 111,, 381–389, 1994.

Tanaka, 1995. Tanaka, T., Generation mechanisms for magnetosphere-ionosphere current systems deduced from a three-dimensional MHD simulation of the solar wind-magnetosphere-ionosphere coupling processes, J. Geophys. Res., 100, 12057–12074, 1995.

Janhunen, 1994-1996. Tela the Tensor Languagea: A scientific computing environment, `http://www.geo.fmi.fi/prog/tela.html`, 1994-1996.

Ogino, 1986. Ogino, T., A three-dimensional MHD simulation of the interaction of the solar wind with the earth's magnetosphere - The generation of field-aligned currents, J. Geophys. Res., 91, 6791–6806, 1986.

Press *et al.*, 1992. Press, W.H., S.A. Teukolsky, W.T. Vetterling, and B.P. Flannery, Numerical Recipes in C: The art of scientific computing, 2nd edition, Cambridge, 1992.

Watanabe and Sato, 1990. Watanabe, K. and Sato, T., Global simulation of the solar wind-magnetosphere interaction - The importance of its numerical validity, J. Geophys. Res., 95, 75–88, 1990.